Available online at www.sciencedirect.com
ScienceDirect
Materials Science and Engineering C 28 (2008) 223–227
MATERIALS SCIENCE & ENGINEERING C
www.elsevier.com/locate/msec

Histomorphologic evaluation of Ti–13Nb–13Zr alloys processed via powder metallurgy. A study in rabbits ☆

M.C. Bottino [a], P.G. Coelho [b,*], M. Yoshimoto [c], B. König Jr. [d], V.A.R. Henriques [e], A.H.A. Bressiani [c], J.C. Bressiani [c]

[a] Department of Materials Science and Engineering, University of Alabama at Birmingham, BEC 254 1530 3rd Avenue South, Birmingham, AL, 35294, USA
[b] Department of Biomaterials and Biomimetics, New York University, College of Dentistry, 345 East 24th Street, Room 804S, New York, NY, 10100, USA
[c] Materials Science and Technology Center, Institute for Energy and Nuclear Research, Av. Prof. Lineu Prestes, 2242, São Paulo, SP, 05508-000, Brazil
[d] Department of Anatomy, Institute of Biomedical Sciences, University of São Paulo (ICB-USP) Av. Prof. Lineu Prestes, 2415, São Paulo, SP, 05508-900, Brazil
[e] Materials Division (AMR/IAE), CTA Brazilian Aerospace Technical Center, São José dos Campos, SP, 12228-904, Brazil

Received 31 March 2006; accepted 5 December 2006
Available online 16 December 2006

Abstract

This study presents the in-vivo evaluation of Ti–13Nb–13Zr alloy implants obtained by the hydride route via powder metallurgy. The cylindrical implants were processed at different sintering and holding times. The implants' were characterized for density, microstructure (SEM), crystalline phases (XRD), and bulk (EDS) and surface composition (XPS). The implants were then sterilized and surgically placed in the central region of the rabbit's tibiae. Two double fluorescent markers were applied at 2 and 3 weeks, and 6 and 7 weeks after implantation. After an 8-week healing period, the implants were retrieved, non-decalcified section processed, and evaluated by electron, UV light (fluorescent labeling), and light microscopy (toluidine blue). BSE-SEM showed close contact between bone and implants. Fluorescent labeling assessment showed high bone activity levels at regions close to the implant surface. Toluidine blue staining revealed regions comprising osteoblasts at regions of newly forming/formed bone close to the implant surface. The results obtained in this study support biocompatible and osseoconductive properties of Ti–13Nb–13Zr processed through the hydride powder route.

Keywords: Titanium alloys; Osseointegration; Biocompatibility; Rabbits

1. Introduction

The word biomaterial comprises a spectrum of natural or synthetic substances that while in temporary or permanent contact with living tissues do not jeopardize their homeostasis [1]. Biomaterial's compatibility is considered to be optimal once tissue neoformation and later function occurs around implantable devices [2].

Cp-Ti and its alloys have been the material of choice for reestablishment of bones' systems in orthopedics and dental rehabilitation. However, while these materials present short- and long-term treatment success, their elastic modulus mismatch relative to bone may potentially lead to localized tissue loss during function [3]. In addition, despite the superior mechanical properties presented along acceptable biocompatibility of Ti–6Al–4V alloy, concerns regarding the release of its elemental constituents such as Al and V have led biomedical researchers to search for potentially more biocompatible alloys [4].

In an attempt to improve on both bone biomechanical and biological response to implants, Ti alloys presenting lower elastic modulus based on chemical elements considered "vital" [5] have been subject of interest. For this reason, Ti–13Nb–13Zr alloys have been developed and tested regarding its chemical, mechanical and in-vivo properties [6,7]. The purpose of this study was to evaluate the in-vivo behavior of Ti–13Nb–13Zr alloy implants processed via powder metallurgy based on the blend elemental hydride method.

☆ Based on a thesis submitted to the graduate faculty, Institute for Energy and Nuclear Research — IPEN (São Paulo, Brazil).

* Corresponding author. Tel.: +1 6468121893; fax: +1 8668219602.
E-mail address: pgcoelho@nyu.edu (P.G. Coelho).

0928-4931/$ - see front matter © 2007 Published by Elsevier B.V.
doi:10.1016/j.msec.2006.12.014

2. Materials and methods

The metallic powders involved in the Ti–13Nb–13Zr (wt.%) alloy processing were obtained by the hydriding method and were sintered in hydride state [8]. After weighing (stoichiometric ratio), blending, and pre-pressing the powders, the green compacts were encapsulated under vacuum and isostatically cold pressed at 300 MPa for 30 s. The samples were then sintered in niobium crucibles under high vacuum (10^{-7} Torr) at three different temperatures and holding times: *Batch (1/B1)* — 1000 °C/5 h, *Batch (2/B2)* — 1300 °C/3 h, and *Batch (3/B3)* — 1500 °C/2 h, at heating rates of 20 °C/min.

Sintered samples' density was determined by measuring the samples' dimensions and weight. X-ray diffraction (XRD) analyses (DMAX 2000, Rigaku, Japan) were performed for crystalline phase identification. Metallographic standard procedures were utilized for microstructural evaluation under scanning electron microscopy (SEM) (Philips XL 30, Eindhoven, The Netherlands) at various magnifications. Alloy composition assessment was performed by EDS (EDAX®, Japan) at various locations. Survey and site specific analysis was performed by X-ray photoelectron spectroscopy (XPS) (Kratos Axis 165 multitechnique, Manchester, United Kingdom).

For in-vivo evaluation, Ti–13Nb–13Zr implants of 6 mm height and 3.2 mm diameter of the three different batches were sterilized according to conventional procedures. Following approval by the Ethics Committee in Animal Research of the University of São Paulo (Institute of Biomedical Sciences), implants were placed at the central region of the tibia of New Zealand rabbits through an anteromedial incision. Implant sites were drilled under low speed (1250 rpm under saline irrigation) through burs of sequentially increasing diameter. The different batches of implants fabricated were press-fit placed into the bone and the soft tissue was closed by standard suture techniques. Antibiotic therapy (Benzilpenicylin at 1.200.00 UI) was carried out during the immediate postoperative period (48 h).

For fluorescent labeling two double labels were applied. Subcutaneous injections of oxytetracycline and calcein-green (10 mg/kg) were administered at 2 and 3 weeks, and 6 and 7 weeks after implantation, respectively. These doses were dissolved in saline solution together with a solution lid of $NaHCO_3$. Eight weeks after surgery, the animals were euthanized by an anesthetic overdose, the limbs retrieved by sharp dissection, and non-decalcified sections were prepared for electron and optical microscopy [9,10].

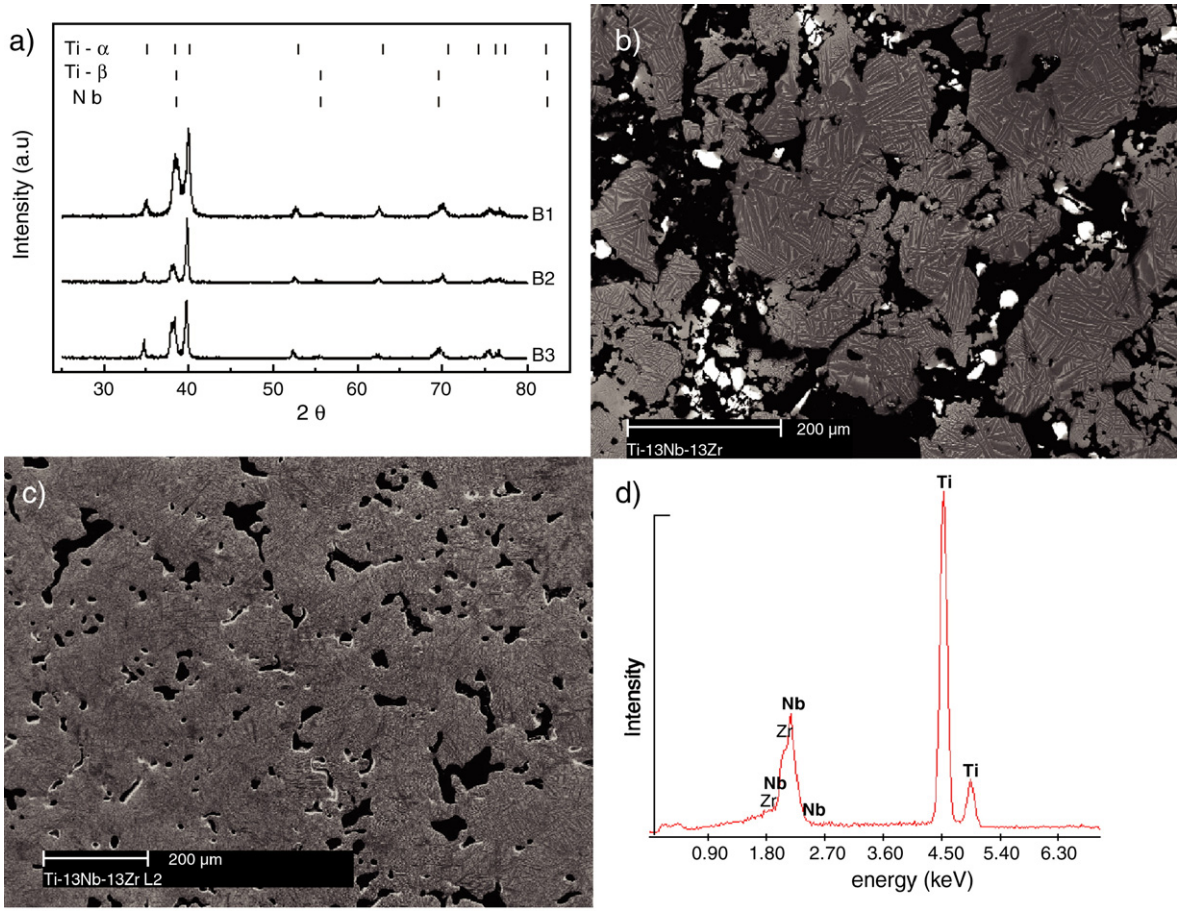

Fig. 1. (a) Typical Ti–13Nb–13Zr spectrum obtained for B1, B2, and B3 samples. (b) BSE-SEM of a B1 (1000 °C/5 h) sample microstructure showing light areas throughout the microstructure comprising undissolved Nb. Note the interconnected pore network. (c) BSE-SEM representative of B2 (1300 °C/3 h) and B3 (1500 °C/2 h) samples showing a more homogeneous microstructure with reduced porosity degrees compared to B1. (d) EDS semi-quantitative chemical composition assessment at various regions of the different samples showed uniform alloy composition for B2 and B3 samples.

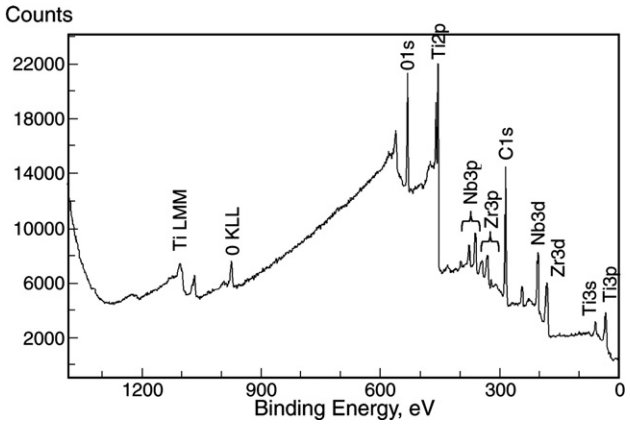

Fig. 2. Survey XPS spectrum showed the presence of Ti and its oxides, Nb, Zr, and adsorbed carbohydrates from the atmosphere at the samples' surfaces.

The non-decalcified samples were evaluated in the as-processed condition for biointegration (SEM) assessment and fluorescent labeling (UV light microscopy). Subsequently, the non-decalcified samples were stained with toluidine blue and evaluated on a light microscope for bone histomorphology.

3. Results and discussion

3.1. Alloy processing

The density values found for B1, B2, and B3 samples presented densification levels of 68%, 88%, and 93% of the 5.01 g/cm^3 density obtained for Ti–13Nb–13Zr samples processed by the arc melting technique [11]. X-ray diffraction (XRD) analysis of the different sintered samples (B1, B2, and B3) showed α and β peaks associated with titanium phases (Fig. 1a). No hydride, oxide, or intermetallic-related phases were detected (Fig. 1a).

BSE-SEM analysis revealed partially dissolved niobium (Nb) areas in localized regions of B1 samples (clear spots on Fig. 1b). Fig. 1b also showed interconnected pore regions obtained at this sintering temperature and holding time ranging from 50 to 100 μm diameter, which is considered appropriate for bone ingrowth [12,13]. More homogeneous microstructures were observed in samples sintered at 1300 °C (B2) and 1500 °C (B3) (Fig. 1c), where a reduction in porosity levels was observed compared to B1 samples.

General semi-quantitative chemical composition assessment through EDS (Fig. 1d) at various regions of the different samples supported that the intended alloy composition was achieved throughout most samples. An exception to that was samples sintered under the lowest temperature (B1), which did not have all Nb dissolved in the microstructure (Fig. 1b). The survey surface chemical analysis assessed through XPS (Fig. 2) showed peaks related to the presence of Ti and its oxides, Nb, and Zr. The surface atomic composition from survey spectra at various locations of the Ti–13Nb–13Zr samples generally showed atomic composition around 22.2% O, 13.5% Ti, 58.0% C, 2.8% Nb, 3.4% Zr. The presence of the carbon peak was due to the presence of carbohydrates from the atmosphere adsorbed onto the alloy surface prior to analysis. No contamination by other elements was observed, which is desirable for biocompatibility of implantable devices.

In summary, the hydride processing route can be regarded as an alternative to other processing technologies available for the production of Ti–13Nb–13Zr alloys. However, attention should be given to sintering temperature and holding time in order to achieve proper alloy homogenization and densification.

3.2. In-vivo aspects

Immediate follow-up after surgical procedures demonstrated no complications regarding procedural conditions, postoperative infection, or other clinical concerns.

3.2.1. Implant osseointegration assessment

SEM micrographs acquired immediately after limbs retrieval showed the presence of mineralized tissue in contact

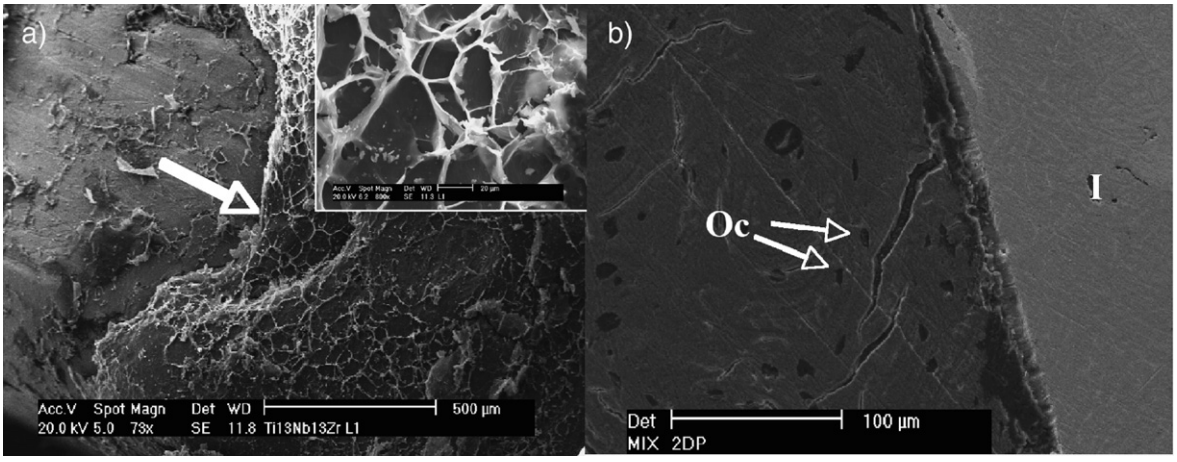

Fig. 3. (a) SEM micrograph acquired immediately after retrieval showing the presence of mineralized tissue in contact with the exposed implant's surface edges. The arrow depicts periosteum remnants (corner detail) after the retrieval procedure. (b) BSE-SEM micrograph showed close contact between bone and implant for all samples. Note the osteocytes' presence in the lacunae (Oc).

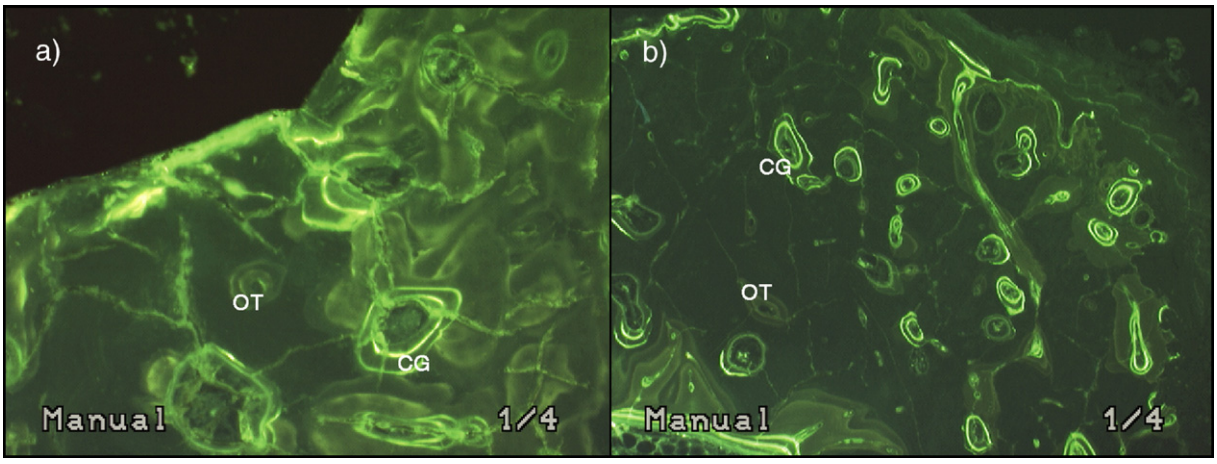

Fig. 4. Fluorescent labels detected for all samples at both cortical and trabecular bone regions. Oxytetracycline (OT) (brown color labels) and calcein-green (CG) (green color labels) were observed at higher amounts at the (a) region immediately adjacent to the implant surface and at lower amounts (100× mag.) at (b) regions away from the implant surface (40× mag.). (For interpretation of the references to color in this figure legend, the reader is referred to the web version of this article.)

with the exposed implant surface edges for all samples. The micrograph presented in Fig. 3a shows the implant partially included in the tibia, as per surgical placement protocol. The arrow depicts periosteum remnants after the retrieval procedure (Fig. 3a). The BSE-SEM micrographs evaluated for all implant batches' non-decalcified sections showed close contact between bone and implant (Fig. 3b). The micrograph presented in Fig. 3b shows the intimate interaction between bone and implant, supporting osseoconductive and biocompatible properties for Ti–13Nb–13Zr alloys processed through the hydride powder method. Also, the presence of osteocytes included in the bone matrix near the implant surface region showed that high bone maturity levels were achieved after 8 weeks in-vivo [10]. The biocompatibility of the alloy processed in this study is likely related not only to its chemical constituents [5], but also due to the presence of a stable layer [10] present in its surface demonstrated by XPS (Fig. 2).

3.2.2. Fluorescent labeling assessment

Fluorescent labels were detected for all samples at both cortical and trabecular bone regions (Fig. 4a–b). Oxytetracycline (brown color labels) and calcein-green (green color labels) were observed at higher amounts at the region immediately adjacent (Fig. 4a) to the implant surface and at lower amounts at regions away from the implant surface (Fig. 4b). This observation is in agreement with data previously reported in the literature [14–16], which depicted a region of high bone activity at regions 1 mm away from the implant surface in various animal models including humans. The evidence of oxytetracycline and calcein-green bone labeling at the interface shows that continuous osteoblastic activity was present at regions close to the implant surface, supporting modelling/remodelling over several weeks in-vivo (Fig. 4a).

It has been suggested that bone modelling and remodelling at regions in proximity to the implant surface are responsible for short- and long-term success of dental and orthopedic devices

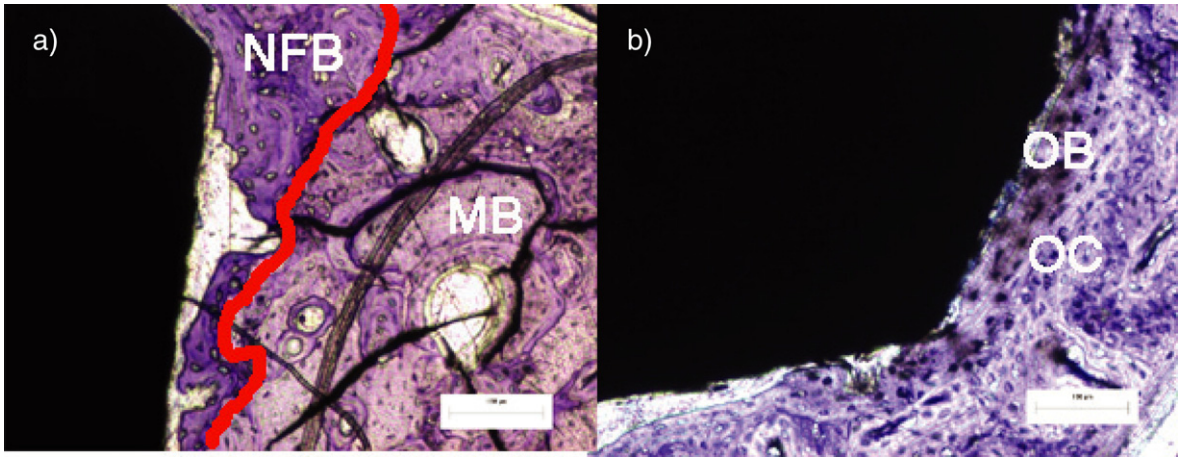

Fig. 5. Toluidine blue stained presented (a) more staining at regions close to the implant surface and less staining at regions away from the implant surface. It should be noted that a sharp transition between newly formed bone (NFB) and mature bone (MB) not affected by surgical trauma was identified in all samples (depicted by red line). (b) Regions comprising osteoblasts (OB) were observed at regions of newly forming/formed bone. All samples showed the presence of newly incorporated osteocytes (OC) in the healing bone area. (For interpretation of the references to color in this figure legend, the reader is referred to the web version of this article.)

[14–16]. Therefore, observation of sustained bone activity levels close to the implant surface over several weeks support high modelling/remodelling kinetics, which will ultimately lead to implant biomechanical fixation due to bone maturation process [14–16].

3.2.3. Toluidine blue staining evaluation

Toluidine bone staining reveals the proteoglycan content of tissues and is a useful tool for identifying regions of mature and immature bone due to their relative differences in organic content [17]. General observation showed that toluidine blue stained samples from different batches presented the same pattern (Fig. 5a–b). This pattern included more staining of regions close to the implant surface and less staining at regions away from the implant surface (Fig 5a). It should be noted that a sharp transition between newly formed bone and mature bone not affected by surgical trauma was easily identified in all samples (Fig. 5a).

A region comprising osteoblasts was observed at regions of newly forming/formed bone close to the implant surface (Fig. 5b). In addition, all samples showed the presence of newly incorporated osteocytes in the healing bone area (Fig. 5b). Osteocytes were also observed at the lacunae of bone regions not affected by surgical trauma (Fig. 5a–b). These results are in agreement with previous in-vivo investigations of Cp-Ti and its alloys [3,10].

4. Conclusion

According to the results obtained, it can be concluded that the hydride powder method route is feasible for production of Ti–13Nb–13Zr devices. The histomorphologic findings presented in this study are in agreement with previous published data concerning in-vivo assessment of Cp-Ti and other titanium alloys including Ti–6Al–4V, supporting biocompatible and osseoconductive properties of Ti–13Nb–13Zr processed by the hydride powder method.

Acknowledgments

This research was financially supported by FAPESP (Brazil) and by CNPq (Brazil).

References

[1] D.F. Williams, Medical and Dental Materials, VCH Publishers Inc., New York, USA, 1992.
[2] L.L. Hench, J. Am. Ceram. Soc. 81 (1998) 1705.
[3] J.E. Lemons, J. Oral Implantol. 30 (2004) 318.
[4] Y. Okazaki, S. Rao, T. Tateishi, Y. Ito, Mater. Sci. Eng., A Struct. Mater.: Prop. Microstruct. Process. 243 (1998) 250.
[5] D. Kuroda, M. Niinomi, M. Morinaga, Y. Kato, T. Yashiro, Mater. Sci. Eng., A Struct. Mater.: Prop. Microstruct. Process. 243 (1998) 244.
[6] S.B. Goodman, L.V. Davidson, Fornasier, A.K. Mishra, J. Appl. Biomater. 4 (1993) 331.
[7] J.A. Davidson, A.K. Mishra, P. Kovacs, R.A. Poggie, Bio-Med. Mater. Eng. 4 (1994) 231.
[8] E.B. Taddei, V.A.R. Henriques, C.R.M. Silva, C.A.A. Cairo, Mater. Sci. Eng., C, Biomim. Mater., Sens. Syst. 24 (2004) 683.
[9] K. Donath, G. Breuner, J. Oral Pathol. 11 (1982) 318.
[10] T. Albrektsson, P.I. Branemark, H.A. Hansson, J. Lindstrom, Acta Orthop. Scand. 52 (1981) 155.
[11] S.G. Schneider, Obtenção e caracterização da liga Ti–13Nb–13Zr para aplicação como biomaterial. Tese de doutoramento. Instituto de Pesquisas Energéticas e Nucleares, São Paulo, 2001.
[12] R.M. Pilliar, Clin. Orthop. 176 (1983) 42.
[13] A.I. Itäla, H.O. Ylanen, C. Ekholm, K.H. Karlsson, H.T. Aro, J. Biomed. Mater. Res. 58 (6) (2001) 679.
[14] E.W. Roberts, L.C. Poon, R.K. Smith, J. Oral Implantol. 12 (3) (1986) 406.
[15] L.P. Garetto, J. Chen, J.A. Parr, W.E. Roberts, Implant Dent. 4 (4) (1995) 235.
[16] P.G. Coelho, M. Suzuki, J. Appl. Oral Sci. 13 (2005) 87.
[17] F. Grizon, E. Aguado, G. Huré, M.F. Baslé, D. Chappard, J. Dent. 30 (5–6) (2002) 195.